ACE-FEDERAL
REPORTERS, INC.

444 North Capitol Street
Washington, D.C. 20001
(202) 347-3700

STENOTYPE REPORTERS

May 2, 1985

TO: The Nuclear Regulatory Commission

IN THE MATTER OF: The Cleveland Electric Illuminating Company, et al
Perry Nuclear Power Plant
Unites 1 & 2
Docket No.: NRC 50-440/50-441
April 30, 1985

Enclosed please find Exhibit 13 of the above referenced proceeding. Please insert the enclosed into your copy of the transcript.

We apologize for any inconvenience this may have caused.

Robert J. Monick

Robert J. Monick

Encl.
NRC: O+5

TR-01
1/1

OCRE E4.13

AES 8211352-1
Final Report

APTECH engineering services, Inc ENGINEERING CONSULTANTS

795 SAN ANTONIO ROAD • PALO ALTO • CALIFORNIA 94303 (415) 858 • 2863

ANALYSIS OF INACCESSIBLE AND POTENTIALLY REJECTABLE DEFECTS IN PERRY NUCLEAR POWER PLANT

Prepared by

Warren P. McNaughton
Geoffrey R. Egan
Jeffrey D. Byron

Aptech Engineering Services, Inc
795 San Antonio Road
Palo Alto, California 94303

Prepared for

Gilbert Associates, Inc.
Post Office Box 1498
Reading, Pennsylvania 19603

Attention: Paul B. Gudikunst

July 19[illegible]

QUALITY ASSURANCE VERIFICATION RECORD SHEET

Title: Analysis of Inaccessible and Potentially Rejectable Defects in Perry Nuclear Power Plant

Originated by: Warren P. McNaughton 5-25-83
Warren P. McNaughton

Jeffrey D. Byron 5-26-83
Jeffrey D. Byron

Verified by: Jeffrey J. Grover 26 MAY 83
Jeffrey J. Grover

Approved by: Geoffrey R. Egan 5-26-83
Geoffrey R. Egan

Quality Assurance Approval: Russell C. Cipolla 5/26/83
Russell C. Cipolla

TABLE OF CONTENTS

TABLE OF CONTENTS
(Continued)

SYNOPSIS

This report summarizes the results of fracture mechanics and fatigue evaluations which were performed for the Perry Nuclear Power Plant Units 1 and 2. These evaluations were performed for several regions of the containment structures as follows:

- Inaccessible locations in weld Joints 1-1 and 2-1 which had weld indications

- Three inaccessible weld locations in Joints 1-4, 1-7, and 1-9

In these last three locations, incomplete radiographic information exists to establish the existing defect size (for example, whether or not full repairs were made); however, sufficient data do exist to characterize the maximum extent of a defect that could remain in the structure and this potential defect has been analyzed.

The evaluations that were performed required three types of input data. These data were stresses, both applied and weld residual stresses, flaw geometries and material properties.

Recently, revised stress data were supplied by Gilbert Associates for the containment. Bounding cyclical and steady state stresses were incorporated to provide an analysis that results in a conservative evaluation of the weld indications. A conservative residual stress determination was also made by assessing the appropriate experimental data.

Flaw data were obtained from radiographic enhancement techniques performed on supplied radiographs. The radiographs provided contain defects which were deemed rejectable according to the criteria of ASME Boiler and Pressure Vessel Code Section III, Subsection NE-5320. These techniques were used to provide accurate sizing of the indications. Such

determinations remove some of the conservatism which has traditionally been used to assess structures with defects in the absence of actual flaw size data.

Material properties such as strength, fracture toughness and crack growth rates were determined using available Certified Material Test Reports and by comparison to generic data obtained from the open literature.

The results confirm that crack growth by fatigue is small over the design plant lifetime, even assuming conservative stress levels, bounding initial flaws and worst case crack propagation rates. Furthermore, it is shown that the applied stress intensity values reached during and after such growth are less than the critical value to cause structural failure. The conservative result of the linear elastic fracture mechanics methodology used in this work is then confirmed using both elastic-plastic and net section collapse (or limit load) methods. It is shown that relatively long and deep flaws can be tolerated even with the conservative assumptions which have been made.

Section 1
INTRODUCTION

A review of radiographs for the Perry Nuclear Power Plant Units 1 and 2, has found certain containment welds that contain potentially rejectable indications, when evaluated per the requirements of ASME Boiler and Pressure Vessel Code Section III, Subsection NE-5320 (1-1). This subsection provides accept/reject conditions based on workmanship standards. The radiographs can be grouped into two logical regions of interest.

The first group of weld indications are found in radiographs associated with weld joints 1-1 and 2-1. These weld locations are inaccessible. They are located in the containment wall (see Figure 1-1) in double sided butt welds and are covered on the inside of the containment by a doubler plate. Indications have been found that would be considered rejectable by ASME Boiler and Pressure Vessel Code, Section III criteria. These radiographs, determined by Level III evaluation to contain rejectable indications, include 21 radiographs of weld 1-1 and 43 radiographs from inaccessile regions in weld joint 2-1 of Unit 2. The weld imperfections on these radiographs were sized using enhancement techniques and conservative interaction criteria. The stresses in Units 1 and 2 are identical, so that bounding defects were developed considering both Unit 1 and 2 indications.

The second group of indications consists of three specific weld locations in joints 1-4, 1-7 and 1-9. Weld joint 1-4 has a defect at location (79-80) 11-12, which has been sized at 2 3/4" long and 1/16" in height. It appears to be a plate delamination (CD-139, Attachment 4).

In weld joint 1-7, at location (110-111) 25-26, the film shows a questionable indication. If this location were accessible the disposition would be to grind and retake. In addition, the film is in question because

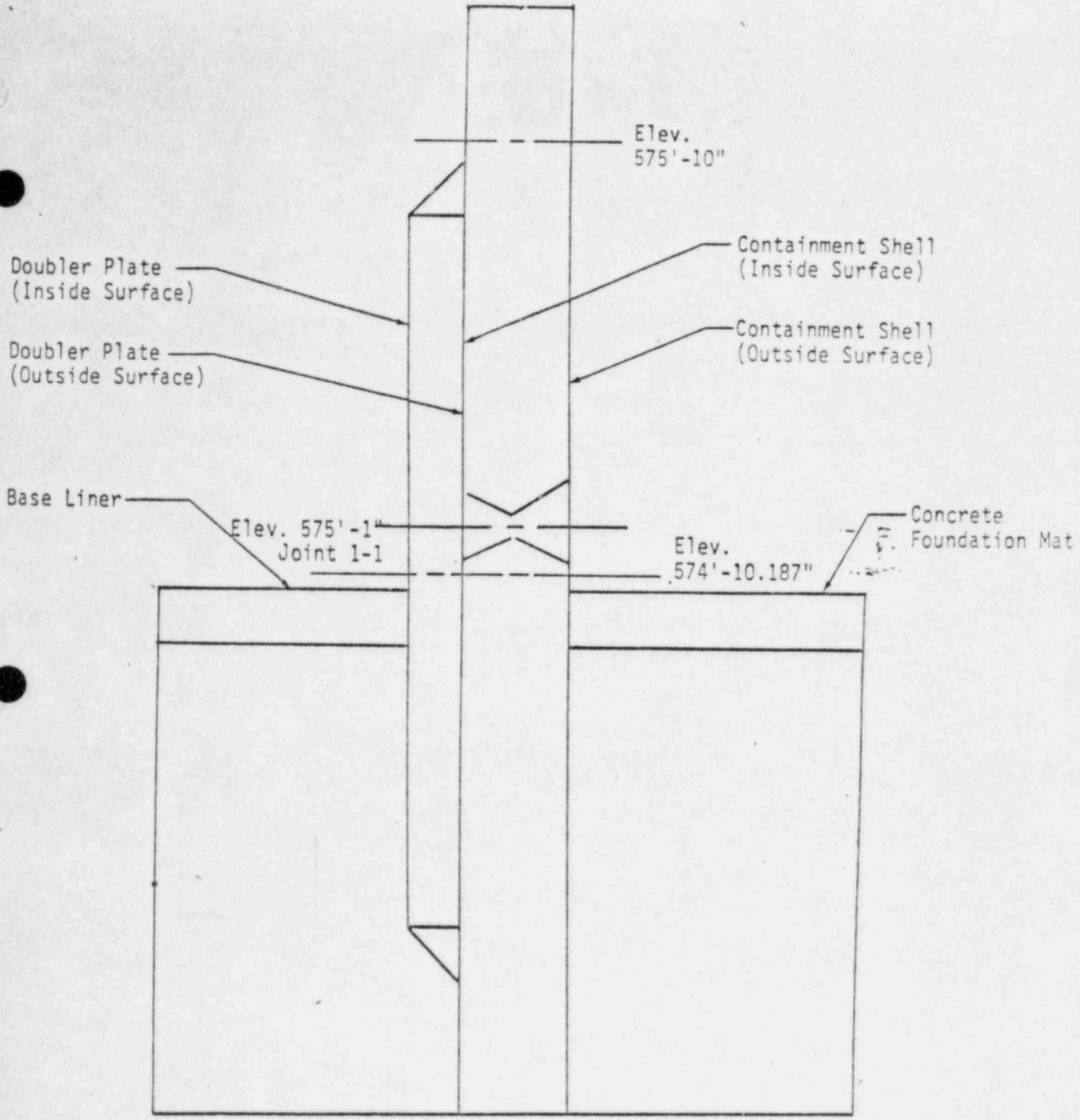

Figure 1-1 Typical Horizontal Weld Joint
(1-1 shown here)

It does not cover the full indication. At maximum, it would be a 9/16" long slag line (CD-139, Attachment 3).

In weld joint 1-9, at location (134-135) 24-25, the film has no indications, however, the adjacent film did have repair which extended into this station. A slag inclusion may still be present, maximum length equal to 1 3/4" (CD-139, Attachment 3). These locations are also inaccessible and the existing radiographic information can be used to provide worst case estimates of defect size remaining in the structure, or of the possible incomplete repairs.

All welds have been fabricated using E7018 weld metal. The defects are completely contained in the weld metal except in joint 1-4 where the indication is in the base material-SA516 Grade 70. The concern in each case is that the indications if unrepaired, may lead to early structural failure. This report addresses that concern and does so by evaluating the potential for defect growth by a fatigue mechanism and concurrent or subsequent failure by fracture.

The remainder of this report consists of six sections. Section 2.0 outlines the analysis methods that have been used to evaluate the defects. The next four sections introduce and discuss input to the analytical model. They are: the evaluation of stresses-both applied and residual (Section 3.0), characterization of material properties (Sections 4.0 and 5.0), and results of the enhancement work performed (Section 6.0). Section 7.0 provides the results of the analysis performed. Conclusions and summary are provided in Section 8.0. Throughout the report, reference is made to documents which have been used to provide input information to the analysis. These documents which are considered controlled under the requirements of the Aptech quality assurance system are designated Controlled Document (CD) and are referenced in Appendix D of this report.

Section 2
ANALYSIS METHODS

The following sections discuss those aspects of fracture mechanics and fatigue theory which were used in the analysis of the present problem. A presentation of general fracture mechanics background (2.1) is followed by a discussion of methods of analysis to assess fatigue growth (2.2).

2.1 Fracture Mechanics Background

The failure behavior of structures under monotonic (slowly increasing) loading can be classified into three regimes in which a specific type of failure mode is appropriate. These three regimes cover brittle fracture, ductile fracture and plastic collapse. The disciplines required to assess these regimes are:

- Linear Elastic Fracture Mechanics (LEFM) - The structure fails in a brittle manner and, on a macro scale, the load to failure occurs within nominally elastic loading.

- Elastic-Plastic Fracture Mechanics (EPFM) - The structure fails in a ductile manner, and significant stable crack extension by tearing may precede ultimate failure.

- Fully Plastic Instability (Limit Load Theory) - The failure event is characterized by large deflections and plastic strains associated with ultimate strength collapse.

A diagram that shows the relationship between critical or failure stress and flaw size for the three failure modes is given in Figure 2-1. The shape and position of the failure locus will depend on the fracture toughness (K_{Ic}) and strength properties (σ_ℓ) of the material, as well as the structural geometry and type of loading.

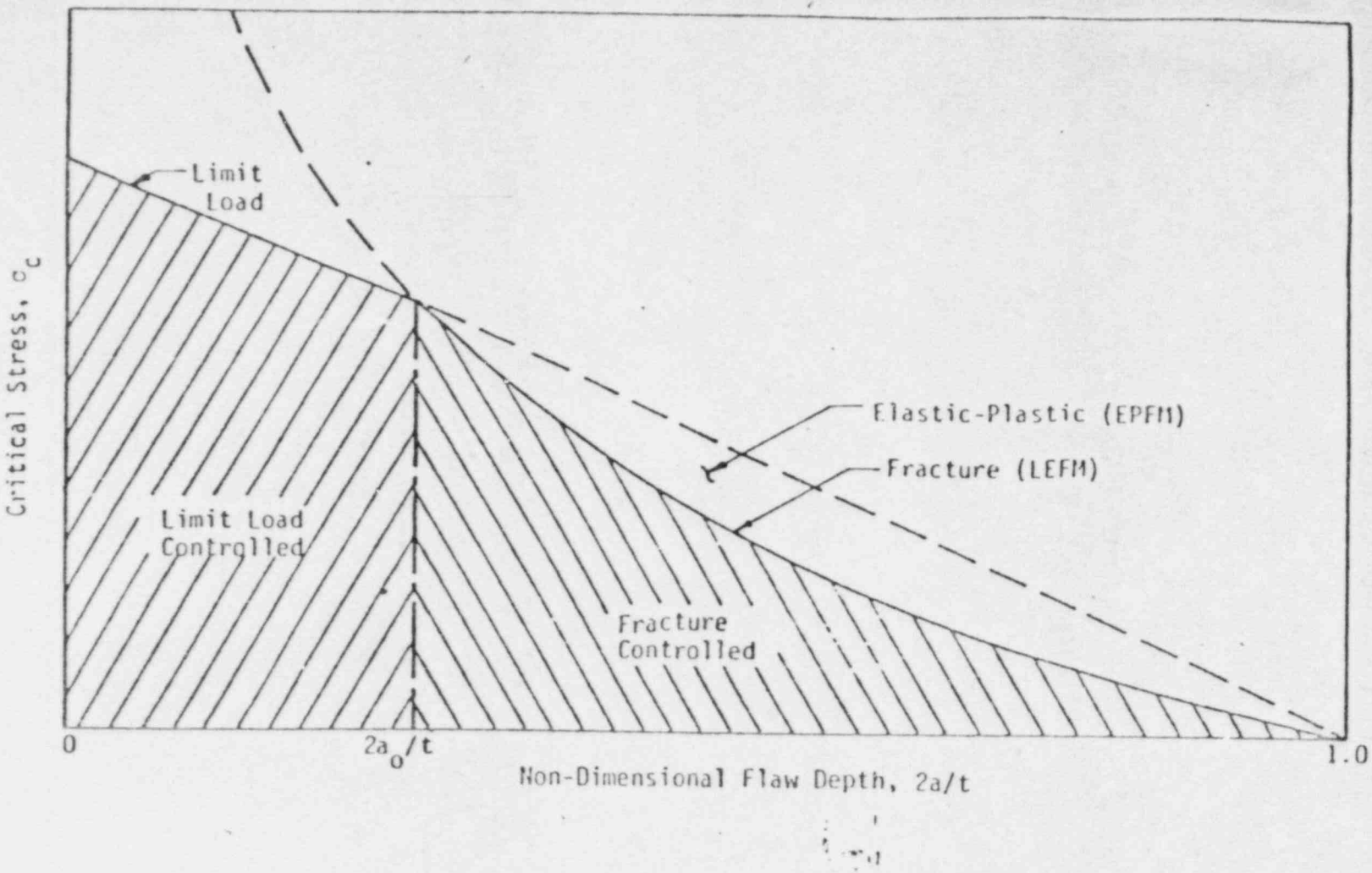

Figure 2-1 Schematic Showing the Relationship Between Failure Stress and Flaw Size For Two Limiting Failure Modes.

2.1.1 Linear Elastic Fracture Mechanics (LEFM)

The principles of linear elastic fracture mechanics (LEFM) are applied to assess quantitatively the conditions for brittle fracture. Brittle fracture consists of two separate events: (1) the initiation of a crack, and (2) the subsequent propagation of the crack to complete failure. Each of these events, initiation and subsequent propagation, has different characteristics. For ferritic structural steels of the SA516 type and carbon manganese weld metal of the E7018 class, the resistance to a propagating fracture is usually lower than the resistance to fracture initiation under slowly applied loads. This is because steels of this type are sensitive to loading rate; the high loading rates associated with a running crack lead to higher yield strength and, hence, lower values of fracture toughness. In constant load situations, therefore, continued crack propagation is expected once the fracture has initiated. For this reason, no attempt is made to evaluate the characteristics of the propagating crack after it has initiated, and the criterion of fracture initiation is used as the definition of failure in the fracture analyses.

Fracture initiation occurs at a defect when the crack driving force exceeds the material's inherent resistance to crack initiation, or fracture toughness. The crack driving force is a function of the stresses acting on the defect and the geometry of the defect. The stresses which act on the defect include both primary (applied) stresses and secondary (internal) stresses. Examples of secondary stresses are residual stresses and thermal stresses that are in equilibrium across the section. The manner in which a structure will fail will be determined by the interaction of the defect geometry, loading, and material toughness.

In linear elastic fracture mechanics, the most useful parameter for characterizing the behavior of cracks is the stress intensity factor K_I, which describes the magnitude of singular stresses ahead of a crack in a linear elastic body loaded in tension. For loading normal to the crack plane (Mode I), fracture initiation occurs when the applied stress intensity factor, K_I, equals or exceeds some critical value, which is

called the fracture toughness of the material. The applied stress intensity factor can be written in the form:

$$K_I = C\sigma\sqrt{\pi a} \qquad (2.1)$$

where σ is the acting stress, a is the characteristic flaw dimension, and C is a parameter which accounts for the flaw shape, structural geometry, and the type of loading. In general, C is a function of a and in many cases must be evaluated numerically. Fracture will occur under quasi-static loading when,

$$K_I \geq K_{Ic} \qquad (2.2)$$

(i.e., when the applied stress intensity factor equals or exceeds the static fracture toughness, K_{Ic}). This means that the occurrence of fracture is controlled by: (1) the stress level, (2) the flaw size, and (3) the fracture toughness. For small flaws, low stresses and high toughness, the applied K will not reach K_{Ic}, and fracture will not occur. These relationships are relevant for material properties determined under plane strain, linear elastic conditions.

To determine the significance of the inaccessible defects in question, it is necessary to know the material fracture toughness, acting stress level and actual distribution of defect sizes and shapes. Knowing any two of these parameters, one can solve for the third. For example, the critical flaw size to cause failure is calculated from:

$$a_c = \frac{1}{\pi C^2}\left(\frac{K_{Ic}}{\sigma_c}\right)^2 \qquad (2.3)$$

if both the toughness (K_{Ic}) and the stress level (σ_c) are known. Conversely, the critical applied stress as a function of crack depth can be computed from,

$$\sigma_c = \frac{K_{Ic}}{C\sqrt{\pi a}} \qquad (2.4)$$

Although these conditions most appropriately describe the behavior of low toughness, high strength materials where little ductility precedes fracture, the use of K_{Ic} as a toughness measure for either SA516 steel or E7018 weld metal ensures a conservative estimate of critical flaw size for brittle fracture, since no account is taken of the increased toughness which results from post-yield (transitional) behavior. Incorporating transitional behavior with more pre-fracture ductility gives increased toughness levels and decreases the susceptibility of the structure to fracture from a given sized flaw. The temperature dependence of toughness properties means that at ambient or higher temperatures, both SA516 steel and E7018 weld metal are above their lower shelf values on a fracture energy versus temperature curve. This in turn implies that the use of standard elastic fracture mechanics will be conservative. Elastic-plastic crack opening displacement (COD) concepts have been used as a check on structural integrity. Elastic-plastic fracture mechanics concepts are discussed in the next section.

2.1.2 Elastic-Plastic Fracture Mechanics (EPFM)

The basic principles of EPFM have been developed over several years (2-1, 2-2, 2-4) and one national standard exists for crack opening displacement (COD) testing (2-5). This method uses critical COD values (as measures of the material toughness) which are not available for the actual field material. A review of the literature (notably 2-6) was made to check the appropriate material characteristics.

One of the best methodologies for EPFM evaluation, the British Standards Institution published document PD6493:1980 (2-7), utilizes crack opening displacement (COD) concepts. In principle, the critical condition is reached when the applied K_I or COD (δ) reaches the resistance level of toughness necessary to cause fracture (K_{Ic} or δ_c). The COD method is completely compatible with the LEFM approach (2-8) and can be used in place

of the K_{Ic} method. For applied stresses well below yield,

$$\delta = \frac{8\epsilon_y a}{\pi} \log_e \sec\left(\frac{\pi}{2} \frac{\sigma}{\sigma_y}\right) \qquad (2.5)$$

where δ is the developed COD; ϵ_y and σ_y are the yield strain and yield stress of the region in which the defect is sited; σ is the applied stress; and a is the half crack length of a center-cracked plate model. It can be seen from Equation 2.5 that as σ approaches σ_y, the developed COD becomes infinite. This only occurs for the elastic-perfectly-plastic material behavior that was assumed for the development of Equation 2.5. For materials that work harden, the relationship between COD and applied strain (for stresses above yield) has been determined by analytical, numerical, and experimental methods (2-9, 2-10).

As in LEFM, once the stresses and material properties have been characterized, it is possible to determine the allowable flaw size to prevent fracture initiation. It is then possible to determine the expected margin of safety between the flaws that may be in the structure and those necessary to cause failure.

2.1.3 Limit Load Analysis

As the size of a critical flaw increases, a regime is entered in which increasing material toughness no longer can prevent initiation of a crack under monotonic loading. The initiation criterion becomes independent of toughness and now becomes a function of the strength properties of the material and the remaining ligament of material. In this regime, a limit load or plastic collapse analysis describes the governing failure mode.

For limit load analysis, the critical stress to cause failure is calculated from an interaction relation common in the analysis of steel structures. This relationship between the applied membrane load (P) and bending moment (M) at failure in a beam or plate with a rectangular cross-section is:

$$\left(\frac{P}{P_\ell}\right)^2 + \left(\frac{M}{M_\ell}\right) = 1 \qquad (2.6)$$

where P and M are the applied loads, and P_ℓ and M_ℓ are the limiting values of P and M. The magnitude of P_ℓ and M_ℓ are functions of crack length a, flaw geometry and material properties.

The limit load of P_ℓ is determined from the geometry of the section and the material properties. After the reduction in area due to the flaw is accounted, the limit load can be expressed in terms of a limit stress and the geometric variables. The limit stress is normally the material yield strength when the material behavior is assumed to be elastic-perfectly-plastic. However, for materials which exhibit significant strain hardening, σ_ℓ could be somewhere between yield and ultimate strength, and the appropriate value to use should be determined by tests.

For this analysis, we use a flow stress which is the average of the yield and ultimate strengths, i.e.:

$$\sigma_\ell = (\sigma_y + \sigma_{uts})/2 \qquad (2.7)$$

where σ_ℓ is the flow stress, σ_y the specified minimum yield stress and σ_{uts} the specified minimum ultimate strength.

Once the limit conditions have been calculated, Equation 2.6 and the expressions for applied membrane stress as a function of pressure and applied moment can be used to determine the failure condition.

A limit load evaluation has been made in conjunction with LEFM methods in the present case.

2.1.4 Summary of Fracture Mechanics Background

The failure behavior of structures under monotonic loading can be

classified into three regimes. Of these, linear elastic fracture mechanics has been determined to be most applicable to the current material and service conditions. Bounding studies based on elastic-plastic and plastic limit load analyses have also been performed.

2.2 Fatigue Loading

2.2.1 Analysis Method

The preceding discussion addressed the case of monotonic loading. In the present case, there are a small number of cyclic loads which may occur on the containment structure. This section discusses the way in which these loads can be evaluated in the light of the previous discussion.

Fatigue evaluation, based on fracture mechanics, assumes that initial flaws are present of size a_i and that the lifetime of a component is that required for a crack to grow from the initial size, a_i, to the critical size, a_c. Crack growth rate data may be correlated to the crack tip stress intensity factor range (ΔK) for the given load cycle in the following form:

$$da/dN = f(\Delta K) \qquad (2.8)$$

where da/dN is the crack growth per load cycle. By integrating Equation 2.8 with the appropriate component stress field to calculate K, the number of cycles, N, (residual life) for a crack to grow from a_i to a_c is computed from:

$$N = \int_{a_i}^{a_c} \frac{da}{da/dN} \qquad (2.9)$$

The final flaw size expected at the end of the design life, a_f, can be determined by integrating Equation 2.8, using the appropriate stress distribution to calculate K, and the number of total design cycles N_o from

$$N_o - \int_{a_i}^{a_f} \frac{da}{da/dN} = 0 \qquad (2.10)$$

where Equation 2.10 is a transcendental expression involving a_f and must be solved by an iterative process.

2.2.2 Crack Growth Rate Representation

Many empirical relations to express da/dN behavior have been proposed; the earliest and most well known is the Paris rule (2-11) which takes the form,

$$da/dN = C\Delta K^n \qquad (2.11)$$

where C and n are constants determined from the data, and ΔK is the range of applied stress intensity factor computed from the minimum and maximum stress in the cycle:

$$\Delta K = \Delta K_{max} - \Delta K_{min} \qquad (2.12)$$

The advantage of the Paris relation is that it is simple in form and it fits experimental data well in the middle range of ΔK. A disadvantage of the relationship is that it does not directly account for mean stress effects (R-ratio effect where $R = K_{min}/K_{max}$) which can accelerate fatigue crack propagation. However, these effects are accounted for in the choice of experimental data used in the modeling procedure.

Section 2
REFERENCES

2-1 Wells, A.A., "Notched Bar Tests, Fracture Mechanics and Brittle Strengths of Welded Structures," Houdremont Lecture 1964, British Welding Journal, No. 1 (January 1965).

2-2 Sumpter, J.D.G. and C.E. Turner, "Fracture Analysis In Areas of High Nominal Strain," Proceedings Second International Conference on Pressure Vessel Technology, San Antonio, TX (October 1973).

2-3 Egan, G.R., "The Application of Fracture Toughness Data to the Assessment of Pressure Vesel Integrity," Proceedings Second International Conference on Pressure Vessel Technology, San Antonio, TX (October 1973).

2-4 Burdekin, F.M. and M.G. Dawes, "Practical Use of Linear Elastic and General Yielding Fracture Mechanics With Particular Reference to Pressure Vessels," Conference on Practical Application of Fracture Mechanics to Pressure Vessel Design, Institution of Mechanical Engineers, London, UK (1971).

2-5 British Standards Institution, "Methods for Crack Opening Displacemént (COD) Testing," (1972).

2-6 Stuber, A., J.Wellman and S. Rolfe, "Eighth Progress Report on Application of the COD Test Method to the Fracture-Resistant Design of Pressure Vessels," for Subcommittee on Effective Utilization of Yield Strength of the PVRC, (February 1980).

2-7 British Standards Institution, "Guidance on Some Methods for

the Derivation of Acceptance Levels for Defects in Fusion Welded Joints," Published Document PD 6493:1980.

2-8 Egan, G.R., "Compatability of Linear Elastic (K_{Ic}) and General Yielding (COD) Fracture Mechanics," Engineering Fracture Mechanics, Vol. 15, (1973).

2-9 Merkle, J., "Analytical Applications of the J Integral," ASTM STP 536, American Society for Testing and Materials, (1972).

2-10 Hayes, D.J. and Turner, C.E., "An Application of Finite Element Techniques to Post-Yield Analysis of Proposed Standard Three-Point Bend Fracture Test Pieces," International Journal of Fracture, Vol. 10, (1974).

2-11 Paris, P.C., M.P. Gomez and W.D. Anderson, "A Rational Analytic Theory of Fatigue," The Trend in Engineering, Vol. 13, No. 1 (January 1961).

Section 3
ANALYSIS OF STRESSES

The analytical model discussed in Section 2 requires as input the characterization of the stress state present in the containment shell courses. This section discusses both the primary and secondary stresses. The primary stresses are the applied stresses associated with dead load and cyclic service stresses. The secondary stresses, in this case, are the residual stresses due to welding.

3.1 Secondary Stresses

The welds under consideration are double sided butt welds. A literature review was performed to characterize the resulting distribution of residual stresses in this type of weld. The weld has stress components transverse to the weld and longitudinal or parallel to the weld, each with through-thickness distributions. A schematic of these applicable distributions is shown in Figure 3-1. For this analysis the flaw location was assumed to be at the centerline of the plate which is the location for the maximum transverse stress. The flaw location was also assumed to be at the location of maximum longitudinal stress. The transverse distribution through-the-thickness will vary as shown in Figure 3-1.

Figure 3-2 shows single sided butt weld residual stress data transverse through the thickness. This figure is a composite of normalized experimental data based primarily on work done by Nordell and Hall (3-1). In their work, the base plate was ASTM A212 Grade B (precursor to SA516 Grade 70) with double-V butt welds of E7018 material. The applicable thicknesses tested were 1 inch and 1 5/8 inches, requiring 12 and 30 weld passes, respectively. The two thicknesses demonstrated similar through thickness transverse stress distributions. Also shown in Figure 3-2 are residual stresses measured by others (3-2, 3-3).

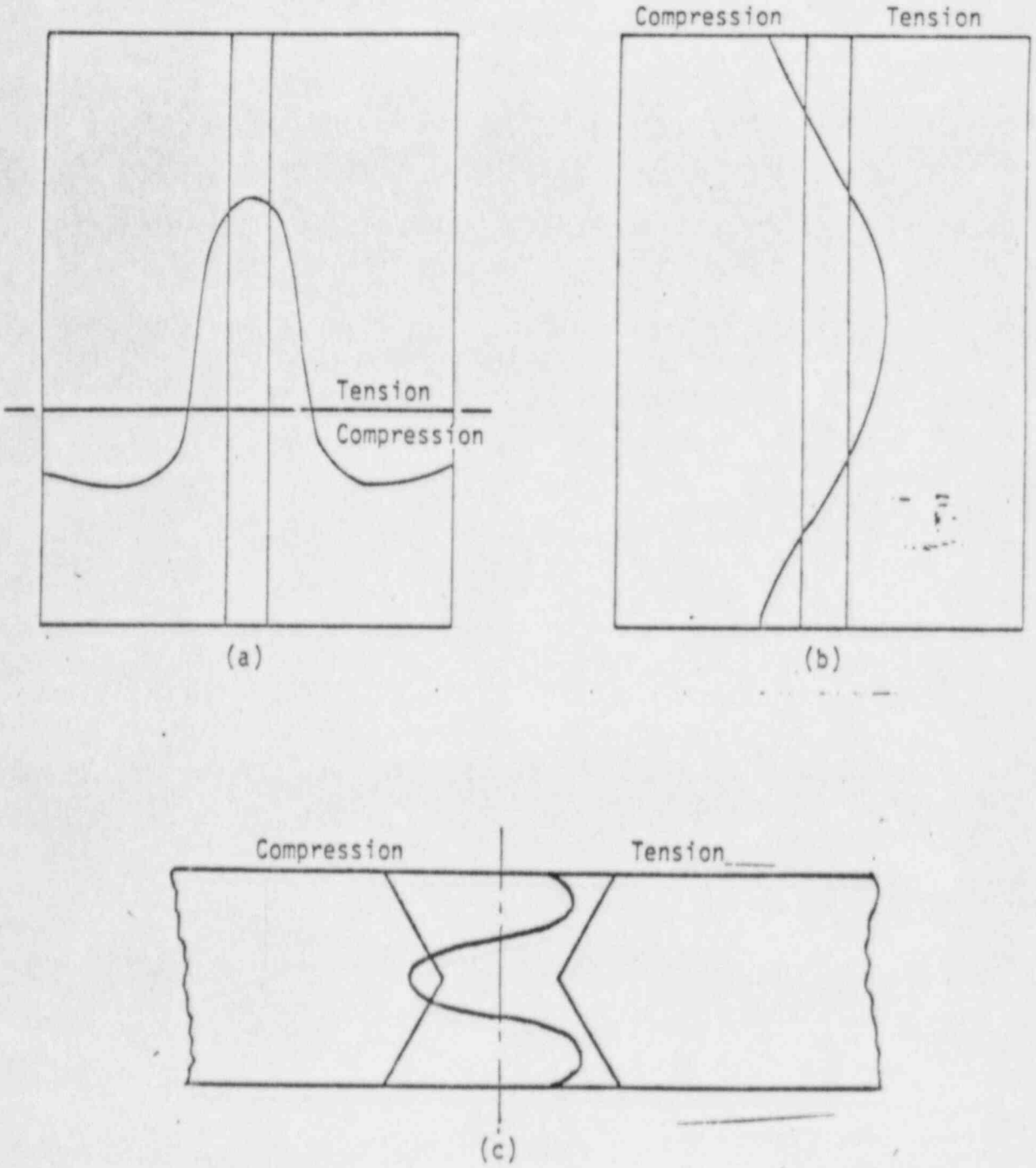

Figure 3-1 Schematic Standard Assumed Residual Stress Distributions in Plates Without Fixed Ends for a Double-Sided Butt Weld: (a) Longitudinal, (b) Transverse, and (c) Transverse Through Thickness.

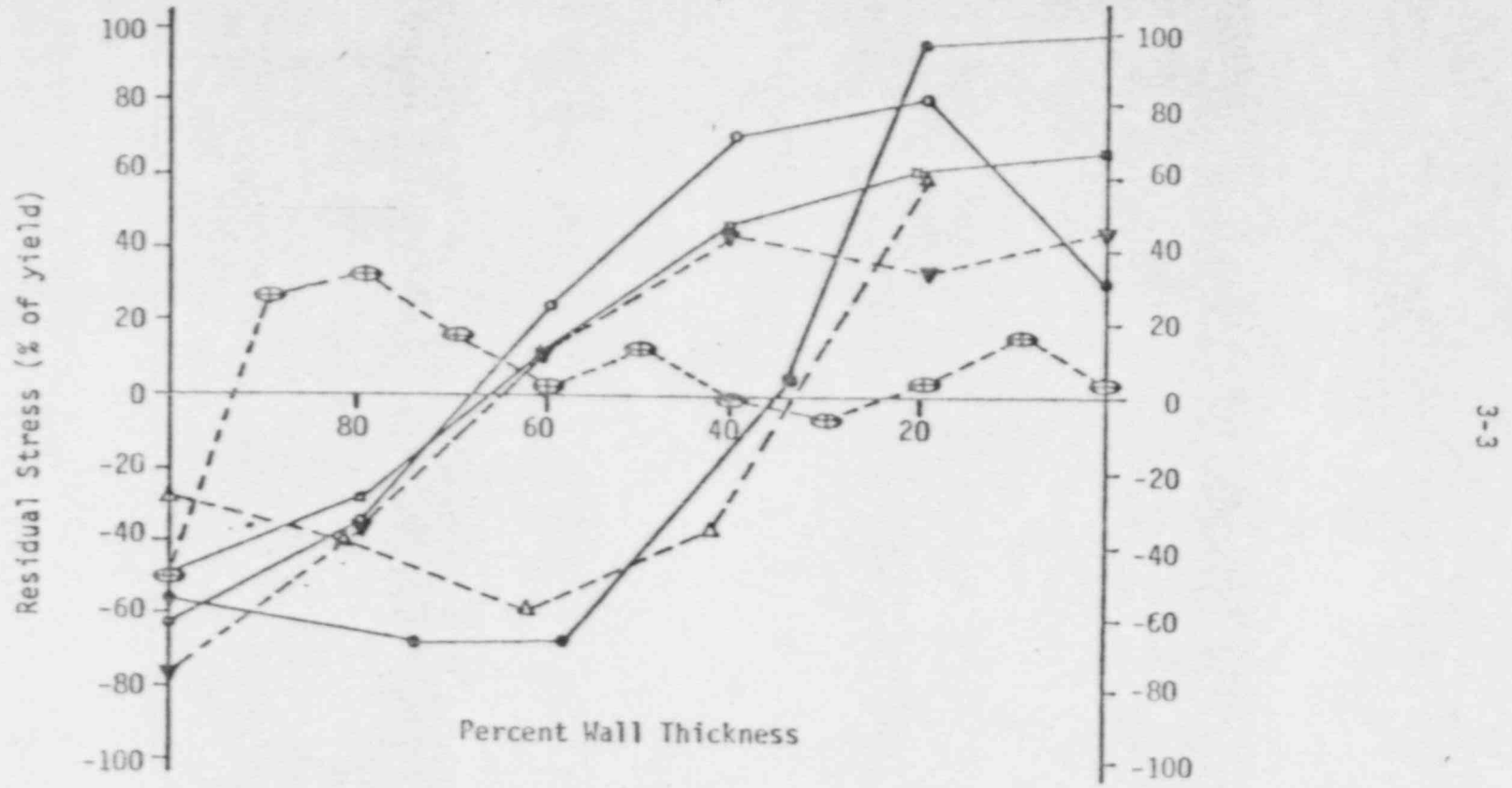

- Nordell and Hall (3-1), 1 5/8" Double V, Piece 1 (half shown)
- Leggatt and Kamath (3-2), 1" Double V, Un-notched (worst half shown)
- Leggatt and Kamath (3-2), 1" Double V, Notched (worst half shown)
- Nordell and Hall (3-1), 1" Double V (half shown)
- Nordell and Hall (3-1), 1 5/8" Double V, Piece 2 (half shown)
- Rosenthal and Norton (3-3), 1" Single V

Figure 3-2 Residual Stresses of Single Sided Butt Welds, Transverse Through Thickness

From these data, a simplified through thickness transverse residual stress distribution was developed. This is shown in Figure 3-3. The distribution assumes yield level residual tensile stresses at the surface through 10% of the thickness. The tensile stresses then decrease to compressive residual stresses equal to one half yield at the mid-thickness. This distribution is then reflected about the centerline of the double sided butt weld to achieve a symmetric and complete distribution. Since any residual stress distribution must be self-equilibrating, the choice of values taken here will be conservative. The sum of the tensile portions is larger than the compressive portions and the maximum values have been assumed uniform except in the through thickness direction.

3.2 Primary Stresses

The primary stresses for analysis have been obtained from unit stress calculations for Joint 1 (CD-130) for welds 1-1 and 1-2; and from Joint 5 (CD-139) for welds 1-4, 1-7, and 1-9. The stresses in welds 1-7 and 1-9 are substantially less than in weld 1-4 (see CD-139 attachment 6). A bounding case has been formulated for welds 1-7 and 1-9 using the stresses in Joint 5 (elevation 592'-2"). These stresses are summarized by Joint number and Load Combination for each Joint and the applicable load combinations. Since the flaws found are oriented parallel to their welds, the stresses in the longitudinal direction apply. A schematic diagram of flaw orientation and applicable stress component is shown in Figure 3-4.

The approach taken was to determine the most highly stressed joint and load combination for the appropriate seam welds. These bounding cases could then be applied to any weld defect, regardless of location, to assure a conservative analysis. In fact, two primary stress distributions were obtained for each weld orientation; one for the fatigue analysis and the other for the fracture analysis.

In order to understand how these stresses were determined, it is necessary to review the tabular stress data as it was provided. Table 3-1 is the

Assumed Double Sided Butt Weld Transverse Through Thickness

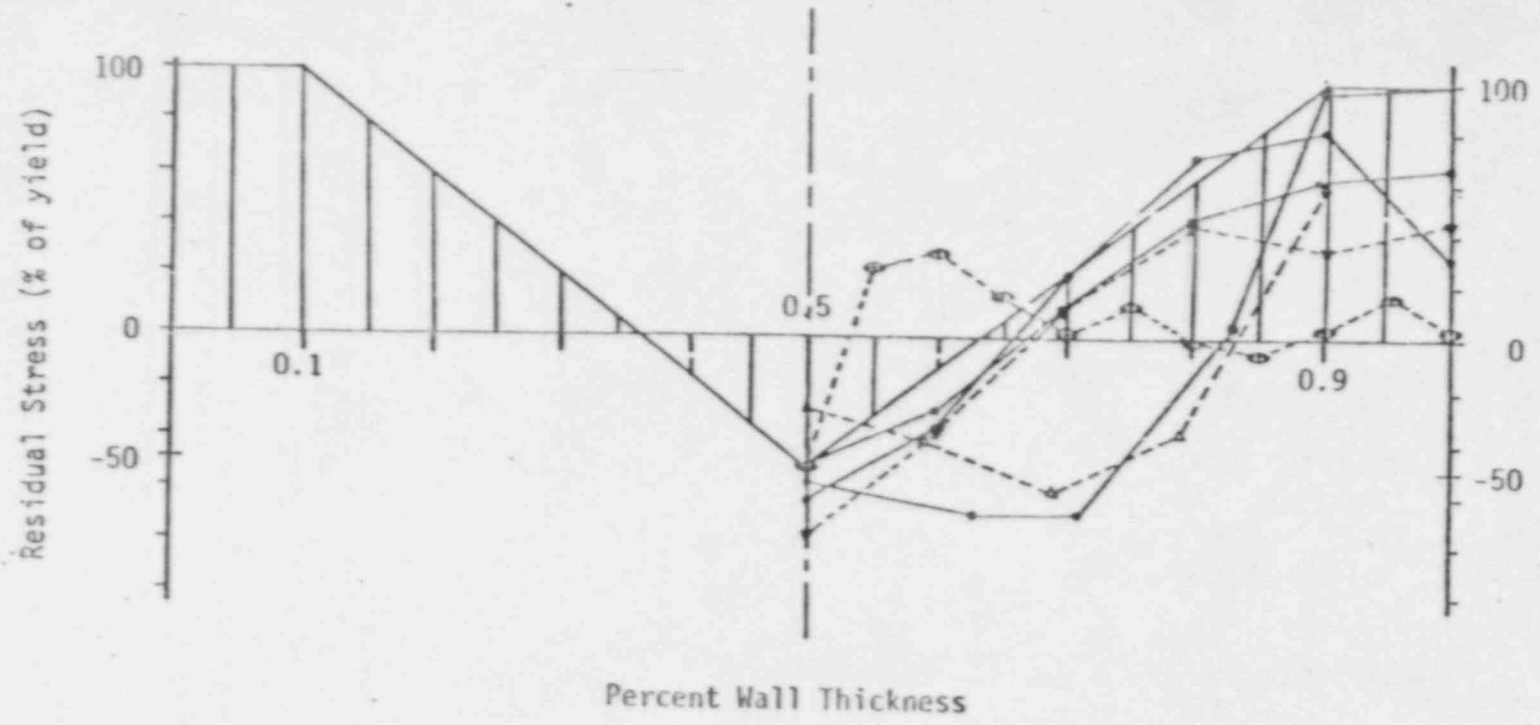

Figure 3-3 Assumed Double Sided Butt Weld Transverse Through Thickness Residual Stress Distribution

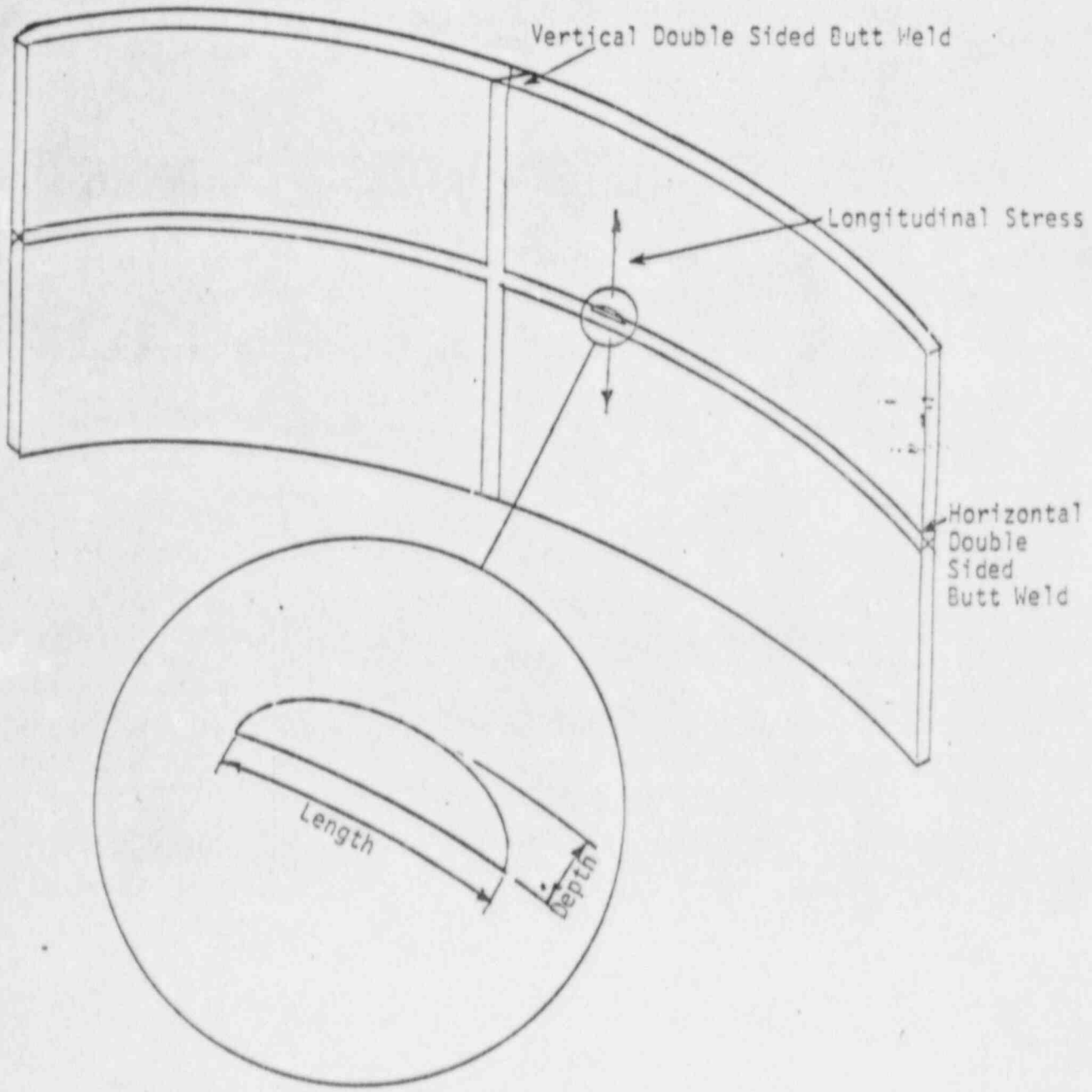

Figure 3-4 Flaw Orientations and Applicable Service Stresses in Vertical and Horizontal Seam Welds

stress summary for Joint No. 5. From this table one can see that the longitudinal and circumferential stresses are broken down into thirteen load components and are then summarized at the bottom of the table into four load combinations. These load combinations represent maximum loading conditions. Some of these load components act at all times, some act cyclically over the life of the plant, and some may act only once. The load components falling into these three categories are summarized in Table 3-2. For a fatigue analysis the cyclic loads are of primary significance and are superimposed with the continuous or steady state loads. For a fracture analysis the most significant loads are those producing the largest stress, which by observation of Table 3-2, are those load combinations that include the single event loads.

Table 3-3 is a summary of the cyclic stresses that govern the fatigue evaluation. There are other cyclic load components. However, the controlling load components in a given load combination are those listed in Table 3-3. Thus, in order to simplify the analysis and provide conservative results, all critical load combinations were evaluated for 16,800 cycles, regardless of which cyclic load components the load combinations include. Table 3-4 shows the appropriate load combination components.

For weld seams 1-1 and 2-1, the stresses taken at Joint 1-1 (elevation 575'-1") were used, as shown in Table 3-5. For welds 1-4, 1-7, and 1-9, weld seam 5 stresses were used to bound the applied stress condition. These primary stress fields were combined with the assumed residual stress field for the analysis.

3.3 Combined Stresses

The total stress considered for the evaluation of a defect consists of the sum of the primary and secondary components. Both sets of stresses have been chosen to bound the expected stress state conservatively. For analytical purposes, they have been superimposed with elastic

Table 3-1

Gilbert Associates, Inc. — CALCULATION

SUBJECT: PERRY NUCLEAR POWER PLANT — JOB — PAGE 4 OF

REV. 1 | 1 | 1 | 1 — MICROFILMED — ORIGINATOR — DATE 2-3-83 — CHECKED — DATE 2/7/83 — PAGE

JOINT NO. 5 EL 592'-2" - CONT. @ 4TH STIFF.

S-PRESS IN PSI

LOAD CASE	LONGITUDINAL - σ_ϕ OUTSIDE	LONGITUDINAL - σ_ϕ INSIDE	CIRCUMF. - σ_2 OUTSIDE	CIRCUMF. - σ_2 INSIDE
DEAD LOAD	-1094.	-389.	-335.	-124.
OPERATIONAL BASE EARTHQUAKE	+/- 1836.	+/- 1836.	+/- 854.	+/- 854.
OBE SLOSH	-41.	42.	-14.	11.
OBE - TILTED POOL	-154.	152.	-42.	50.
Σ a + b + c	+1641 / -2031.	+2030 / -1642.	+798 / -910.	+915 / -793.
SAFE SHUTDOWN EARTHQUAKE	+/- 2704.	+/- 2704.	+/- 1260.	+/- 1260.
SSE SLOSH	-82.	84.	-28.	22.
SSE - TILTED POOL	-464.	475.	-176.	162.
Σ a + b + c	+2138 / -3270.	+3263 / -2145.	+1106 / -1414.	+1444 / -1076.
EXTERNAL HYDROSTATIC LOAD DUE TO ANNULUS CONCRETE POUR	68.	-67.	-463.	-503.
15 PSIG STATIC INTERNAL PRESSURE	-454.	7625.	570.	2994.
SRV DISCHARGE - 19 VALVES	+/- 493.	+/- 456.	+/- 221.	+/- 66.
SRV DISCHARGE - ONE VALVE, 1ST POP	+/- 209.	+/- 274.	+/- 129.	+/- 20.
SRV DISCHARGE - 1 VALVE SUBSEQUENT	+/- 361.	+/- 469.	+/- 224.	+/- 33.
MEAN CONDENSATION OSCILLATION	+/- 31.	+/- 27.	+/- 13.	+/- 5.
MEAN CHUGGING	+/- 42.	+/- 43.	+/- 18.	+/- 8.
HYDROSTATIC PRESSURE 18'6"	-81.	80.	-34.	14.
LOCA POOL SWELL	-6813.	8264.	-1136.	3400.
DBA LOCA THERMAL STRESS	-11413.	8461.	-22183.	-16221.
Σ of ① ② ④ ⑦ ⑪ ⑫	-6072 / -10160.	10142. / 5972.	-1044 / -3007.	3727. / 1974.
Σ of ① ③ ④ ⑦ ⑪ ⑫	-5575 / -11399.	11425. / 5469.	-733. / -3511.	4251. / 1691.
Σ of ① ② ④ ⑤ ⑥ ⑩ ⑪	-615. / -4127.	9778. / 5108.	-775. / -1411.	3270. / 1514.
Σ of 1 2 4 5 8 10 11 13	-10930 / -15408.	18282 / 13556.	-2405 / -23997.	42284 / 14674.

+ TENSION.
- COMPRESSION.

Table 3-2

CLASSIFICATION OF LOAD COMPONENTS BY FREQUENCY OF OCCURRENCE

Continuous or Steady State Loads

Dead Load

External Hydrostatic Load Due to Annulus Concrete Pour

Hydrostatic Pressure 18'-6"

Cyclic Loads

OBE

SSE

SRV Discharge - 19 Valves

SRV Discharge - One Valve, 1st Pop

SRV Discharge - One Valve, Subsequent

Mean Condensation Oscillation

Mean Chugging

Single Load Events

LOCA Pool Swell

DBA LOCA Thermal Stress

15 psig Static Internal Pressure

Table 3-3
SUMMARY OF CYCLIC STRESSES

SOURCES	NUMBER OF OCCURRENCES	NUMBER CYCLES PER OCCURRENCE	TOTAL NUMBER OF CYCLES
SRV Actuation	1860	9	16,740
OBE	5	10	50
SSE	1	10	10
TOTAL			16,800

Table 3-4
LOAD COMBINATIONS EVALUATED FOR ANALYSIS

Load Combination Number	Load Components
I	DL + OBE + CONC + SRV_1 + HYDRO + PS
II	DL + SSE + CONC + SRV_1 + HYDRO + PS
III	DL + OBE + CONC + SIP + SRV_{19} + CHUG + HYDRO
IV	DL + OBE + CONC + SIP + SRV_2 + CHUG + HYDRO + LOCATHERM

DL = Dead Load

OBE = Operating Basis Earthquake

SSE = Safe Shutdown Earthquake

CONC = External Hydrostatic Load Due to Annulus Concrete Pour

SIP = 15 psig Static Internal Pressure

SRV_{19} = SRV Discharge - 19 Valves

SRV_1 = SRV Discharge - One Valve, First Pop

SRV_2 = SRV Discharge - One Valve, Subsequent Pop

CHUG = Mean Chugging

HYDRO = Hydrostatic Pressure 18'-16"

PS = LOCA Pool Swell

LOCATHERM = DBA LOCA Thermal Stresses

Table 3-5

BOUNDING SERVICE STRESSES FOR JOINT 1-1

Location	Stress (psi) Inside	Outside
Stress Component		
Thermal	633	-5857
Hydrostatic	421	-818
Design Pressure	2794	836
Dead Load	-492	-659
PSRV	1085/-1847	-2078/8639
CO	146	279
SSE	±731	±2194
OBE	±555	±1664

Load Combination	Stress Range (psi)	
I	1569/-2473	-1891/498
II	1805/-2709	-1361/-32
III	4509/175	-776/1055
IV	5142/808	-6633/-4802

(From CD-130) Gilbert Ref. Letter PY-STR-1555

perfectly-plastic material behavior.

The cyclic (primary or service) stresses are added to the residual stress distribution such that the maximum stress does not exceed the assumed yield stress of the material. The yield stress used for developing this distribution is 78.6 ksi (see Section 5).

Section 3
REFERENCES

3-1 Nordell, W.J. and W.J. Hall, "Two Stage Fracturing In Welded Mild Steel Plates," Welding Research Supplement, March 1965, Pp. 124-S to 134-S.

3-2 Leggatt, R.H. and M.S. Kamath, "Residual Stresses In 25 mm Thick Weld metal COD Specimens In the As-Welded and Locally Compressed States," The Welding Institute, Report 145/1981, June 1981.

3-3 Rosenthal, D. and J.T. Norton, "A Method of Measuring Triaxial Residual Stresses In Plates," Welding Research Supplement, May 1945, Pp. 295-S to 307-S.

Section 4
FATIGUE CRACK GROWTH RATES

In order to estimate the maximum extent of crack growth that could occur at an indication over the design life of the plant, a fatigue evaluation was performed. This evaluation combined the cyclic stresses (Section 3) with the appropriate crack propagation rates (Section 4) to obtain the expected crack growth (Section 7).

The purpose of this section is to assess propagation rates for defect growth by a fatigue mechanism. With the exception of the possible plate defect in weld joint 1-4, the defects are located in weldments, thus requiring an evaluation of carbon steel weld material crack growth data. References have been drawn together to estimate a conservative (that is fastest possible) bound on potential crack growth. Although no data are available for the exact condition in effect, significant studies have been performed to permit bounding values to be estimated.

The following engineering unit conventions are in effect unless otherwise stated:

- ΔK (stress intensity factor range), ksi $\sqrt{in}$
- T (temperature), °F
- da/dN (crack growth rate), inches/cycle

All weldments evaluated are composed of E7018 weld metal. Data available in the literature were collected for all types of carbon steel weld metal with an emphasis on E7018. A study by Maddox (4-1), resulted in a substantial amount of crack growth data for four different weld metals including E7018. The four types of test specimens from Maddox are

summarized in Table 4-1 and the crack growth data for these specimens are plotted in Figure 4-1. Crack growth data for the E7018 weld material (weld metal C) are shown separately in Figure 4-2. Also shown on Figure 4-1 is the bounding line from similar testing on plain steels performed by Gurney (4-2).

Other data from similar weld metals (4-3) with and without stress relief, fall within the upper bound shown in Figure 4-1 for Gurney (4-2). The literature also states that weld metals for joining steels such as A516 Grade 70 exhibit slower fatigue growth rates than the base metals (4-4).

Residual stresses may increase crack growth rate (da/dN), but if these stresses are included in estimating crack growth rates, the data indicate that the bounding line by Gurney (4-2) will conservatively predict crack growth for E7018 weldments. Figure 4-3 shows Gurney's upper bound which is represented by:

$$da/dN = 2.63 \times 10^{-10} \Delta K^{3.44} \qquad (4.1)$$

The lamination-like defect in weld 1-4 may propagate in either weld material or SA516 Gr. 70 base plate material depending on the exact defect location and orientation relative to the weld. Both cases were analyzed to bound the possible effects. The growth rate used for SA516 Gr. 70 material was derived in previous work for Gilbert Associates (4-5), based on bounding curves developed from work by Bamford (4-6), and ASME Code Section XI (4-7). This work provides a three point curve depending on the relevant cyclic stress range.

$$da/dN = 3.8 \times 10^{-10} \Delta K^{3.76} \qquad \Delta K < 4.9$$

$$da/dN = 4.4 \times 10^{-13} \Delta K^{8.0} \qquad 11 > \Delta K > 4.9$$

$$da/dN = 3.16 \times 10^{-6} \Delta K^{1.4} \qquad \Delta K > 11$$

Table 4-1

TEST SPECIMENS FROM MADDOX*

WELD METAL	AWS/ASTM CLASSIFICATION	YIELD STRESS (ksi)	ULTIMATE STRESS (ksi)	
A	None	74.4	88.0	A MIG deposit using CO_2 gas shielding and 1 mm diameter wire Type A-17 to BS 2901, Part 2, 1960.
B	E7013	68.3	73.9	A manual metal arc deposit of medium strength using a BS 1719 Class E317-rutile coated electrode.
C	E7018.G	67.2	82.9	A manual arc deposit of medium strength using a BS 1719 Class E614 HJ low hydrogen electrode.
D	E9018.G	89.6	105.3	A manual metal arc deposit of high strength made using a BS 1719 Class E614 HJ low hydrogen electrode.

*Ref. (4-1)

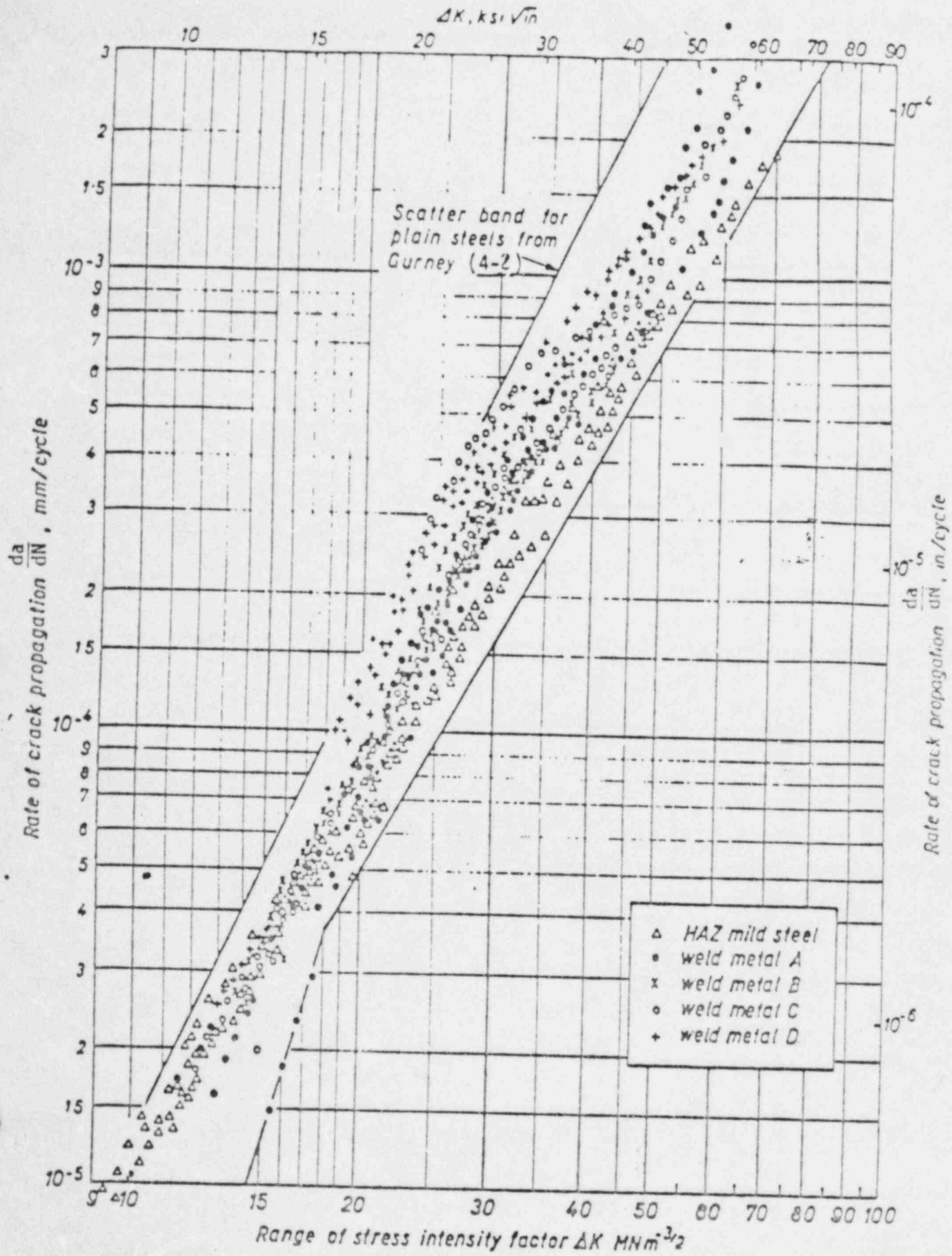

Figure 4-1 Crack Growth data from Maddox (4-1)

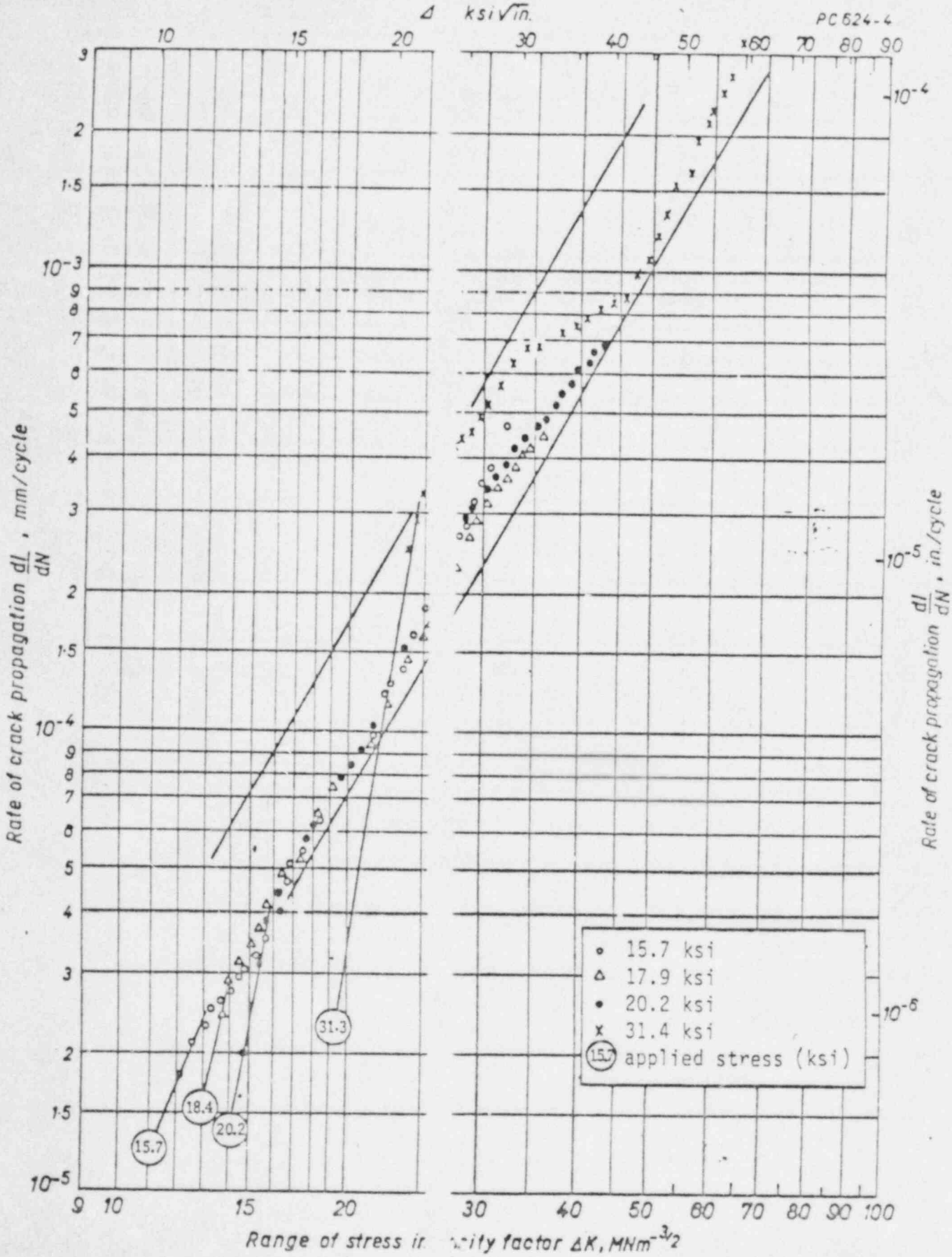

Figure 4-2 Crack gr th data for E7018 from Maddox (4-1)

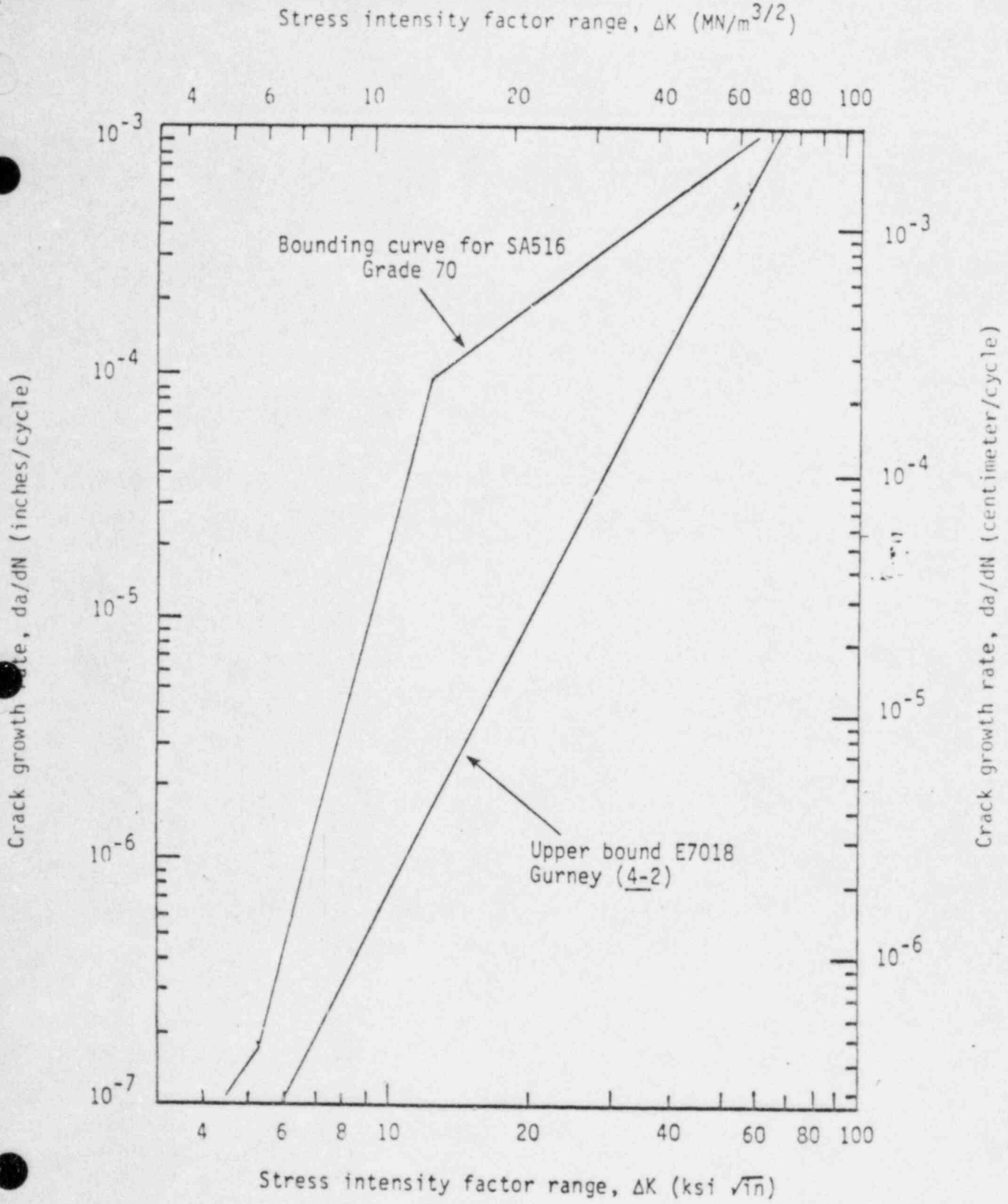

Figure 4-3 Bounding Crack Growth Lines for E7018 weld metal and SA516 Grade 70 base material

These values are shown in Figure 4-3. It should be noted that this curve is very conservative relative to all experimental data reviewed and will provide even more conservative results than the weld metal curve also shown in Figure 4-3.

Section 4
REFERENCES

4-1 Maddox, S.J., "Fatigue Crack Propagation in Weld Metal and Heat Affected Zone Material," The Welding Institute, Report No. E/29/69, Abington, Great Britain, 1969.

4-2 Gurney, T.R. and S.J. Maddox, "A Reanalysis of Fatigue Data for Welded Joints in Steel," The Welding Institute, Welding Research International, Vol. 3, No. 4, 1973.

4-3 Seeley, R.R., L. Katz and J.R.M. Smith, "Fatigue Crack Growth in Low Alloy Steel Submerged Arc Welds," Fatigue Testing of Weldments, Pp. 261-284.

4-4 Gurney, T.R., "An Investigation of the Rate of Propagation of Fatigue Cracks in a range of Steels," The Welding Institute Members' Report No. E18/12/68.

4-5 Egan, G.R., et. al., "The Significance of Sensitized Stainless Steel Material in Drywell Vent and Containment Structures in the Perry Nuclear Power Plant - Fracture and Fatigue Evaluations," AES Report 81-11-88, November, 1981.

4-6 Bamford, W.H., "Application of Corrosion Fatigue Crack Growth Rate Data to Integrity Analysis of Nuclear Reactor Vessels," American Society of Mechanical Engineers, Paper No. 79-PVP-116, 1979.

4-7 American Society of Mechanical Engineers, Boiler and Pressure Vessel Code, Section XI.

Section 5
FRACTURE TOUGHNESS AND STRENGTH

5.1 Introduction

Two additional model inputs to be discussed are the material properties; fracture toughness and strength. As discussed in Section 2, the applied stress intensity is compared to a critical value which is defined as the fracture toughness. Thus, to determine allowable flaw sizes, the fracture toughness must be characterized. Although no direct measurements of fracture toughness were performed in the course of this work, inference about the level of fracture resistance inherent in the material can be made by reference to the Charpy impact values which are available. The background is presented in Section 5.2. The data are discussed in Section 5.3 for the containment welds and base plates (for possible plate delamination of weld 1-4). Section 5.4 analyzes typical crack opening displacement values to be used in the elastic-plastic fracture mechanics evaluation. Section 5.5 addresses the yield and ultimate strength values to be used in the limit load assessment. Certified Material Test Reports (CMTR's) (CD-4, CD-7, and CD-1Z7) were analyzed to determine Charpy (CVN), yield strength and tensile strength data. Controlled document 1Z7 was provided specifically to confirm the CMTR's for E7018 used in Weld Joint 1-1 between seams 21-22 where the largest defects occurred. CD-4 and CD-7 were obtained in previous work for Gilbert and list data for many heats of E7018 used in containment welds. These data have also been included (see Table 5-1) to indicate the variation in material properties.

5.2 Fracture Toughness: Background

To use the analyses described in Section 2.0, it is necessary to have the appropriate value of material fracture toughness in terms of the critical plane strain stress intensity factor (K_{Ic}). Because of the excellent toughness in this material, these data are not normally available for weld metals such as E7018 at temperatures around 70°F. Valid K_{Ic} data for

Table 5-1

SUMMARY OF WELD PROPERTIES BY HEAT
(AS-WELDED)

WELD WIRE QC#	CMTR#	YIELD STRENGTH (σ_y) (KSI)	LIMIT STRESS (σ_c) (KSI)	AVERAGE CVN (FT/LBS)	TEMP. (°F)
77NNI518	456	66.3	72.3	77.3	-30
77NNI540	472	78.1	83.2	69.8	-30
77NNI563	493	63.4	70.3	45.0	-30
78NNI004	552	68.8	75.7	82.6	-20
78NNI013	557	65.8	72.0	95.2	-20
78NNI014	557	68.4	74.3	109.6	-20
78NNI015	557	65.3	69.9	24.0	-20
78NNI016	557	65.5	71.4	85.0	-20
78NNI024	625	65.3	69.9	24.0	-20
*78NNI100	596	78.1	80.7	62.0	-20
78NNI163	630	68.2	73.1	76.0	-20
78NNI164	630	63.8	69.0	115.3	-20
78NNI202	646	66.9	71.5	120.2	-20
78NNI221	653	68.1	73.9	86.8	-40
*78NNI224	655	66.3	72.6	101.0	-20
78NNI255	663	70.2	73.6	118.4	-20
79NNI016	694	84.9	89.8	66.7	-20
79NNI017	694	78.6	83.3	92.7	-20
79NNI018	694	67.2	72.7	114.0	-20
79NNI099	710	64.5	71.3	84.6	-20
79NNI100	710	70.9	76.4	102.4	-20
79NNI131	716	72.7	79.2	80.3	-20
79NNI161	729	65.3	71.5	56.8	-20
79NNI172	737	65.3	71.5	56.8	-20
80NNI017	746	74.8	79.5	81.0	-20
80NNI050	752	70.0	77.0	69.0	-20
*76NNI182	224	68.9	74.9	42.3	-30
*76NNI218	256	68.5	74.3	85.7	-30
*77NNI058	398	70.0	73.8	138.0	-30
*77NNI519		69.0	73.8	113.3	-30
*77NNI589	520	69.7	73.7	109.7	-30

Taken from CD-4 and CD-7

* Included in CD-127

1.5" thick material are generally only available at temperatures such as -100°F. However, it is possible to infer information about the relative toughness of the present material from available CMTR's. There are several correlations that have been proposed to relate Charpy energy to K_{Ic} values. These include two empirical relationships proposed and verified by Barsom and Rolfe (5-1). The relationship for the transition temperature regime is:

$$\frac{K_{Ic}^2}{E} = 2\,(CVN)^{3/2} \qquad (5.1)$$

where

K_{Ic} = Plane strain fracture toughness (psi $\sqrt{In}$)
E = Young's modulus (psi)
CVN = Charpy V-notch energy (ft-lbs)

The corresponding relationship for the upper shelf regime is:

$$\left(\frac{K_{Ic}}{\sigma_y}\right)^2 = \frac{5}{\sigma_y}\left(CVN - \frac{\sigma_y}{20}\right) \qquad (5.2)$$

where

σ_y = Material yield strength (ksi)
K_{Ic} = Plane strain fracture toughness (ksi $\sqrt{In}$)

Barsom and Rolfe found that at 80°F, the upper shelf correlation was appropriate for all material they tested. All their tests were with material of yield strength greater than 100 ksi, although they claim that Equation 5.2 is valid for materials with yield strength less than 100 ksi if dynamic yield strength is used instead of static yield strength.

Another common correlation, due to Sailors and Corten, which was developed for A533B and A517F (5-2), is

$$K_{Ic} = 15.5 \, (CVN)^{0.5} \qquad (5.3)$$

where

K_{Ic} = ksi $\sqrt{in}$
CVN = ft-lb

Pisarski (5-3) who reviewed and verified by experiment ten correlations including those listed above, found that good predictions can be obtained for high strength steels (σ_y > 113 ksi). For lower strength steels, the correlations tend to be generally conservative with the degree of conservatism increasing with decreasing yield strength. Thus, either Equation 5.1 or 5.3 should provide conservative estimates of critical fracture toughness. As a check, relations between critical crack opening displacement value and K_{Ic} are also available from Rolfe and Barsom (5-4) and Egan (5-5), and take the form:

$$\frac{\delta_c}{\varepsilon_y} = \left(\frac{K_{Ic}}{\sigma_y}\right)^2 \qquad (5.4)$$

where

δ_c = Critical crack opening displacement (in.)
ε_y = Yield strain (in/in) = σ_y / E
K_{Ic} = Critical fracture toughness (ksi $\sqrt{in}$).
σ_y = Yield Strength (ksi)

A further evaluation of typical crack opening displacement (COD) values is found in Section 5.4.

5.3 Toughness Values for Containment Welds

Specific certified material test reports (CMTR's) were reviewed only for weld 1-1 between vertical joints 21-22 (CD-127). Furthermore, CMTR's for Perry containment stiffener welds fabricated using E7018 were evaluated in earlier work by APTECH (5-6). These weld data are considered

representative of those that would be found elsewhere in the containment.

There is a large scatter of Charpy V-notch (CVN) data as shown in Table 5-1. The range of test values represented there is 24.0 to 138.0 ft-lbs. The values given for CVN in the table are the "average." This is the average the 5 data points listed in the CMTR or 3 data points if 3 data points are given. In order to be conservative, the lowest CVN value was used to determine fracture toughness (K_{Ic}) of the weld material. Thus, the 24 ft-lbs corresponds to a Barsom-Rolfe toughness value of 82.6 ksi $\sqrt{In}$. With the exception of this one heat, all other heats have calculated K_{Ic} values greater than 132.3 ksi$\sqrt{In}$.

These values represent tough welds, particularly since the CVN tests were performed at a maximum temperature of -20°F, well below the operating temperature. This fracture toughness value of 82.6 ksi$\sqrt{In}$ will be conservative since:

- The Barsom-Rolfe correlation used to arrive at these values has been shown to be conservative for materials with these strength levels.
- Most calculated K_{Ic} values using this correlation are substantially above this level.
- The test temperature used to evaluate K_{Ic} is -20°F, whereas a higher temperature during operation will result in correspondingly higher toughness.

A lower bound determination of SA516 Gr. 70 toughness expected in the containment structure was performed in previous work for Gilbert Associates (5-7). This value was found to be 73.2 ksi $\sqrt{In}$. The derivation of this result involves considerable conservatism.

Other values determined from Table 5-1 to complete the analysis are yield strength and limit stress. The yield stress is used in determination of residual stresses, as they are a function of yield strength level. The higher the yield strength of the material, the higher the residual stresses. Therefore, the upper bound yield strength is used to determine the maximum possible residual stresses present. The limit strength is used in evaluating the limit load capacity of the structure. The limit strength (σ_ℓ) is defined as

$$\sigma_\ell = (\sigma_y + \sigma_{uts})/2 \qquad (5.5)$$

where σ_y is the yield strength and σ_{uts} is the ultimate strength. For conservatism in the limit load analysis, lower bound values for yield and ultimate strength are used in the determination of the limit strength.

For yield stress, a value 78.6 ksi has been used and for limit stress, 66.0 ksi. (See Section 7.2) The conservatism is apparent in that the prescribed yield stress is 12 ksi greater than the limit stress used in the analysis.

5.4 Crack Opening Displacement (COD) Values

Crack opening displacement testing is used as a direct measure of fracture resistance. Literature data are available to provide typical COD values for E7018. These are presented in Appendix A. These data were used in two ways. First, as a check in the derivation of K_{Ic} and second, as direct input to the EPFM analysis.

A check on derivation of the K_{Ic} value used can be provided by Equation 5.4. From the data in Appendix A, the lowest COD value data at 32°F is .023". For this value of COD, and for $\varepsilon_y = 0.2\%$, $\sigma_y = 63.4$ ksi (the lowest strength material given in Table 5-1), the resulting K_{Ic} value is calculated as:

$$\frac{\delta_c}{\varepsilon_y} = \left(\frac{K_{Ic}}{\sigma_y}\right)^2$$

$$K_{Ic} = 214.9 \text{ ksi } \sqrt{\text{in}}$$

Thus, the value of 82.6 ksi$\sqrt{\text{in}}$ taken in Section 5.3 corresponding to a CVN value = 24 ft-lbs., is very conservative.

Section 5
REFERENCES

5-1 Barsom, J.M. and S.T. Rolfe, "Correlations Between K_{Ic} and Charpy V-Notch Test Results in the Transition Temperature Range," ASTM STP 466, (1970), Pp. 281-302.

5-2 Sailors, R.H. and H.T. Corten, "Relationship Between Material Fracture Toughness Using Fracture Mechanics and Transition Temperature Tests," ASTM STP 514, (1973), Pp. 164-191.

5-3 Pisarski, H.G., "A Review of Correlations Relating Charpy Energy to K_{Ic}," The Welding Institute Research Bulletin, (December 1978), Pp. 362-367.

5-4 Rolfe, S.T. and J.M. Barsom, Fracture and Fatigue Control in Structures: Applications of Fracture Mechanics, Prentice-Hall (1977).

5-5 Egan, G.R., "Compatibility of Linear Elastic (K_{Ic}) and General Yielding (COD) Fracture Mechanics," Engineering Fracture Mechanics, (1973), Vol. 5, Pp. 167-185.

5-6 Egan, G.R., W.P. McNaughton and J.D. Byron, "A Fracture Mechanics Analysis of Containment Stiffener Flange Welds in the Perry Nuclear Plant," APTECH Report, AES-82-01-92 (April 1982).

5-7 Egan, G.R., et. al., "The Significance of Sensitized Stainless Steel Material in Drywell Vent and Containment Structures in the Perry Nuclear Power Plant - Fracture and Fatigue Evaluations," AES Report No. 81-11-88, November, 1981.

Section 6
CHARACTERIZATION OF FLAWS

The final input required for the fracture mechanics evaluation is flaw size. The applied stress intensity factor calculated by linear elastic fracture mechanics methods and the net section stress of the limit load method will both require an accurate description of flaw dimensions. This will include both depth and length information. Length information is generally easier to obtain as the projection of length onto film is obtained by standard radiographic methods. Depth data have been less easily obtained without resort to volumetric examination by ultrasonic techniques or destructive testing techniques. For structural integrity evaluations an assumption has been generally imposed that confines the flaw depth to one weld pass in multipass welds for certain defect types. This assumption will be conservative for porosity and slag inclusion defect types. However, in many instances it may be overly conservative. Such an assumption confining the expected defect depth to one weld pass will not however guarantee conservatism for "linear" defects like cracks, lack of fusion and lack of penetration. To more fully characterize both types of defects in the weld joints of interest, a radiographic enhancement technique has been used. This is discussed in Section 6.3 below. The enhancement procedure also allows accurate length sizing of defects. When combined with equations of interaction (discussed below), this allows the analyst to determine if two adjacent defects or a series of defects should be most accurately represented as single imperfections or treated as continuous. The details of defect interaction are discussed in Section 6.2. The following section discusses the effect on structural integrity of the rounded defect types, particularly slag inclusions.

6.1 The Effect of Slag Inclusions on Structure Integrity

Work by Harrison (6-1) has indicated that slag inclusions have little effect on the tensile strength of butt welds up to considerable percentages

of cross-sectional area. In support, he shows results of work by Ishii (6-2) and by Kihara (6-3). These results are shown in Figure 6-1. Harrison further points out that by their nature slag inclusions are unlikely to occupy a large proportion of the cross-sectional area of a given weld and the weld metal will usually overmatch the base metal in strength. The conclusion to be drawn from these factors is that the effect of slag inclusions on static tensile strength in materials like E7018 is negligible. Harrison confirms that size-for-size, slag inclusions will be less detrimental than cracks because of their roundness and limitations on their through-thickness size.

A simillar conclusion is reached considering low cycle fatigue. Work by Ishii and Iida (6-4) is shown in Figure 6-2 and indicates that slag inclusions have little effect on load-controlled low-cycle fatigue and up to lives of about 10^4 cycles. The design can thus be based on the static tensile behavior. For the analysis of these inaccessible defects, the structure may be subjected to as many as 18,600 cycles. This is still considered low-cycle fatigue for the purposes of our analysis, and the effect of slag inclusions will be well characterized by the static loading case, particularly in light of the relatively low magnitude of the cyclic stresses (relative to the fully reversed limit level stresses used to generate the S-N curves of Figure 6-2). Additional results given in figures 6-3 though 6-5 indicate the effects on fatigue strength for high cycle fatigue. The number of cycles required to enter a regime characterized by substantial effects on life is shown to be at least an order of magnitude greater than the design life in the present case.

In summary, Harrison (6-1) states that there seems to be sufficient evidence to indicate that under load-controlled conditions, low-cycle fatigue is not a problem which will be influenced by the presence of slag inclusions.

The tensile strength, σ_u, of a defective butt weld will be either

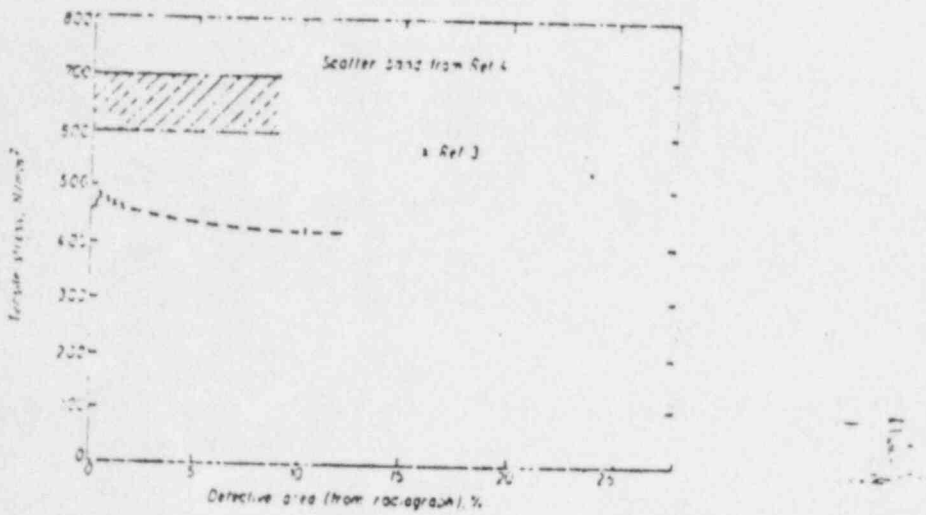

Figure 6-1 Effect of Slag Inclusions on Tensile Strength (taken from 6-1)

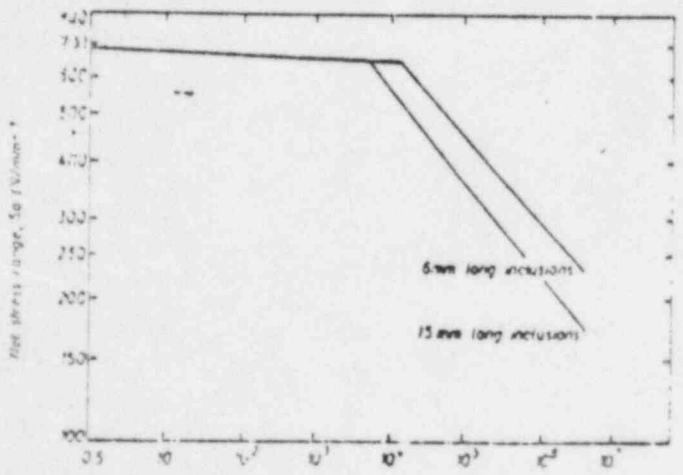

Figure 6-2 Results of Load-Controlled Repeated Stress Fatigue Tests on Butt Welds Containing Slag Inclusions (taken from 6-1)

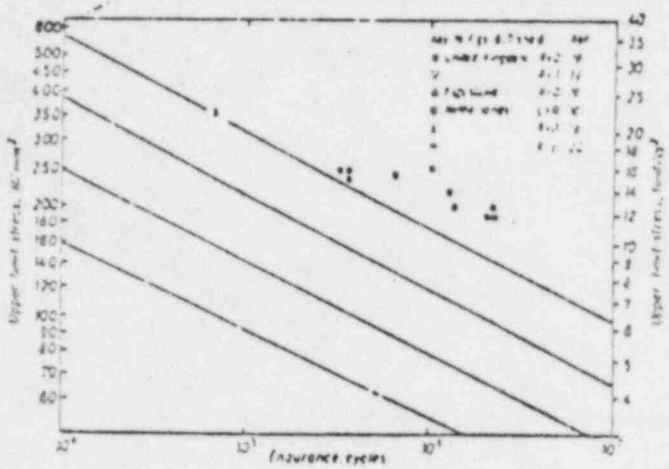

Figure 6-3 Results of Tests on Low-Hydrogen Welds Containing Slag Inclusions up to 5mm Long (taken from 6-1)

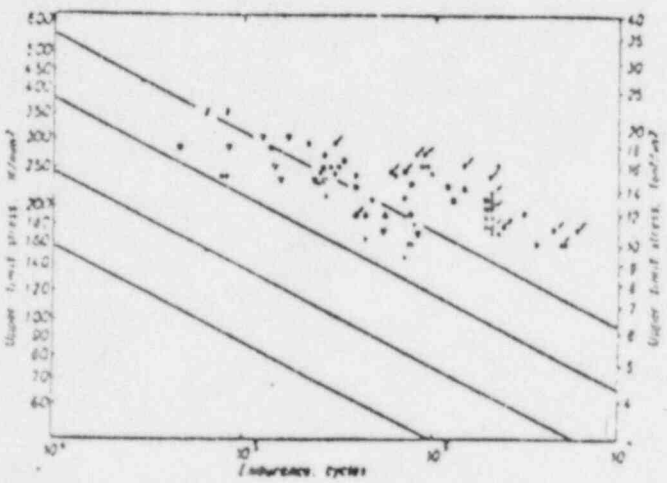

Figure 6-4 Results of Tests on Low-Hydrogen Welds Containing Containing Slag Inclusions up to 25mm Long (taken from 6-1)

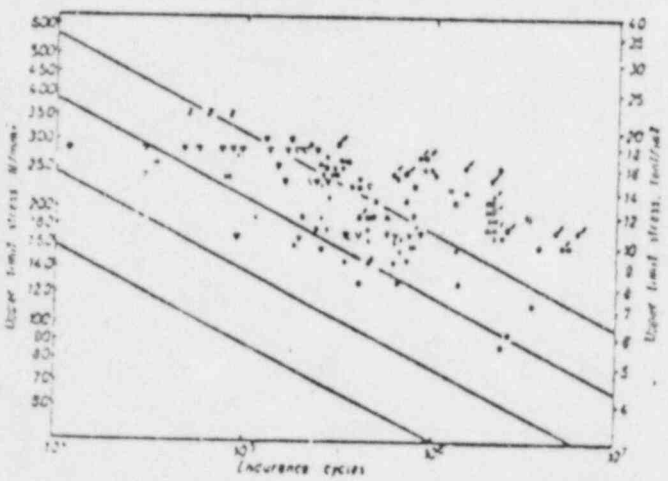

Figure 6-5 Results of Tests on Low-Hydrogen Welds Containing Slag Inclusions up to Continuous Slag Lines (taken from 6-1)

$$\sigma_{u,w} \quad (1 - \Delta A/A)$$

or $\sigma_{u,p}$

whichever is least. Where:

$\sigma_{u,w}$ = the tensile strength of the weld metal

$\sigma_{u,p}$ = the tensile strength of the parent material

$\Delta A/A$ = ratio of the loss of area due to porosity or slag inclusion to the total area

The effect of porosity on structural integrity is similiar to that for slag inclusions. Figure 6-6 shows the effect on tensile strength of a weld as a function of volume of pores. This figure is from work by Harrison (6-5). Figure 6-7 shows the effect on fatigue life for porosity defects for the case of low cycle fatigue. The behavior is similiar to that for slag inclusions. Harrison concludes for porosity (6-5) that, "There seems to be sufficient evidence to indicate that, under load controlled conditions, low cycle fatigue is not a problem which will be influenced by practical porosity levels." Furthermore:

> "In view of the probable necessity to limit porosity to some percentage probably well below 10% because higher levels would obscure other defects, there is no need to give further consideration to the effect of porosity on static ductile strength. This is because weld metals normally overmatch parent material strength and even where this is not the case the percentage reduction in strength due to porosity is equal to the percentage by volume of porosity and at a maximum of 10% this would not in any normal circumstances be significant."